의학석사 학위논문

Magnetic Nanoparticles-Induced Assembly with Endothelial cells for Vascularization

자성 나노 입자로 유도된 혈관 내피 세포와의 어셈블리를 활용한 혈관화 연구

2023 년 2 월

서울대학교 대학원
의과대학 협동과정 줄기세포생물학과

석 호 동

의학석사 학위논문

Magnetic Nanoparticles-Induced Assembly with Endothelial cells for Vascularization

자성 나노 입자로 유도된 혈관 내피 세포와의 어셈블리를 활용한 혈관화 연구

2023 년 2 월

서울대학교 대학원
의과대학 협동과정 줄기세포생물학과

석 호 동

Magnetic Nanoparticles-Induced Assembly with Endothelial cells for Vascularization

자성 나노 입자로 유도된 혈관 내피 세포와의 어셈블리를 활용한 혈관화 연구

지도 교수 황 석 연

이 논문을 의학석사 학위논문으로 제출함

2022년 12월

서울대학교 대학원
의과대학 협동과정 줄기세포생물학과
석 호 동

석호동의 의학석사 학위논문을 인준함

2023년 2월

위 원 장	권성근	(인)
부위원장	황석연	(인)
위 원	박태현	(인)

Abstract

Magnetic Nanoparticles-Induced Assembly with Endothelial cells for Vascularization

Hodong Seok

Interdisciplinary Program of Stemcellbiology

The Graduate School of Medicine

Seoul National University

Engraftment is crucial for cellular survival and the functions of transplants in tissue engineering. When an organ deficit has occurred due to genetic or acquired reasons, organ transportation or cell therapy is a possible treatment. Vascularization around a transplant is significant for the transplant to have long-term viability. To construct a blood vessel-rich environment, vascularization strategies are needed. This study attempted to promote vascularization after transplantation by assembling endothelial cells around spheroids using magnetic nanoparticles

(MNPs) and magnetic force. MNPs were extracted from Magnetospirillum sp. AMB-1 that are biocompatible and spontaneously uptake by cells. The spheroids made by a mouse myoblast C2C12 in this study were intended to represent general organoids. HUVEC was assembled around the spheroid to facilitate vascularization. Briefly explaining the assembly method, C2C12 cells with 20 μg/mL MNPs were seeded on a round bottom ultra-low attachment (ULA) plate which was stacked on neodymium magnets and incubated for 2 days to form the spheroid. MNPs-treated HUVECs were added to the spheroids and assembled around the spheroids on magnets for 1 day. MNPs-internalized HUVECs showed no inhibition of vascularization-related gene expressions. The assembly sprouted their vessel around the spheroid on Matrigel. Finally, the assembly which was transplanted into the murine kidney rapidly engrafted within 3 days, its transplantation resulted in vascularization in the murine hindlimb. This magnetic assembly system is expected to be used as a universal technology for the rapid engraftment and vascularization of transplants.

Keyword: Engraftment, Vascularization, Cellular Assembly, Magnetic Nanoparticles, Transplantation, 3D Cultures, Cell Therapeutics
Student Number: 2021-21331

Table of Contents

List of figures

Chapter 1. Introduction

1.1. Study Background

Transplantation is one of the final goals in tissue engineering. Recently, researches on cell therapeutics for the purpose of transplantation have been actively conducted.[1] In particular, cell therapy is mainly made for transplantation in the form of a three-dimensional structure such as spheroid or organoid.[2-4] Long-term survival of transplanted 3D structures is important to replace defective body parts.[5, 6] Engraftment means that the transplant can communicate properly with other components around it such as the original organ, so it is needed to create a blood vessel-rich environment.[7] A blood vessel network shoul be formed to receive oxygen and nutrient for long-term functioning in the host body.[8] There are two major issues on transplantation, immune and vascularization. Type 1 diabetes also has that issues and is even a disease that inhibits angiogenesis, so the conditions of engrafrment are more difficult.[6, 9, 10] Diabetic diseases are accompanied by a variety of complications, including diabetic foot, for reasons of anti-vasculrization, which makes them more vulnerable to immune responses and requires a lot of effort to survive the transplanted islet.[11-13] In previous study, nanofilm for preventing immune response on islet in type 1 diabetic mouse showed block of tumor necrosis factor α (TNF α) and natueal killer T cells.[14] Now

that the immue response has been resolved, the remaining challenge is the vascularization of the tranplant. There are various strategies of vascularization for transplantation.[5] Using angiogenic factors, porous scaffold, pre-vascularization, and endothelial cells co-aggregation is the examples of strategies of vascularization. We choose entothelial cells assbly for constructing vessel-rich environment.

In order to replace the function of the organ after transplantation, cells that are transplanted need to exist in a 3D structure to mimic the organ rather than exist in itself. So there are so many methods to establish 3D culture. One of them is assbly of cells with magnet[15-17]. This magnetic assembly methods are used to make assembly of one kind of cells including spheroid, and assembly of various kinds of cells including assembloid. In this study, we use magnetic nanoparticles as tool for assembly with endothelial cells for efficienct engraftment. For stable and effective implantation, angiogenesis must be done quickly within 3 days.[18-22] This study focused on the development of a universal assembly system representing various cell therapeutics.

The MNPs used in this study are extracted from Magnetospirillum magneticum, also called AMB-1[23, 24]. AMB-1 is a kind of magnetotactic bacteria (MTB) which produces magnetic nanoparticles called magnetosome inside of their cytosol for survival[25-27]. MTB which live in the water use magnetosomes as compasses which identify their location and determine the direction to move[28]. MNPs from MTB have property of

spontaneously intake to cells because of their thin lipid layer[29, 30]. Uptaken MNPs are placed in endosomes of cell so the cell have magnetism[31]. Because of the magnetism from MNPs, cells can be moved by magnets so spacially applied[16, 32-35].

1.2. Purpose of Research

We are going to suggest a system of assembly various spheroids with endothelial cell using magnetic nanoparticles. Our goal is rapid engraftment within 3 days of spheroids after transplantation. When cell therapeutics including spheroids, organoids, or tissues transplanted, the transplants need efficient engraftment for their long-term survival and functionality. Vessel-enriched environments help to provide oxygen and nutrients to the transplants. However, in the case of diseases such as diabetes that inhibit angiogenesis or ischemia which are lack of vessels, it is not only difficult to build a blood vessel-rich environment, but also the surrounding blood vessels may not be connected to the transplant. Therefore, we focused on the assembly with endothelial cells for engraftment. It was expected to stabilize quickly after transplantation by forming in which sprouting endothelial cells assembled on cell therapeutics with actively form vasculogenesis rather than passive angiogenesis. We aim as a final goal to vascularize pancreatic beta cells in type 1 diabetic models and thereby produce long-term insulin secretion as an advanced form of previous studies. Furthermore, we expect that this magnetic assembly technology will be applied universally to the engraftment of various cell therapeutics transplantation.

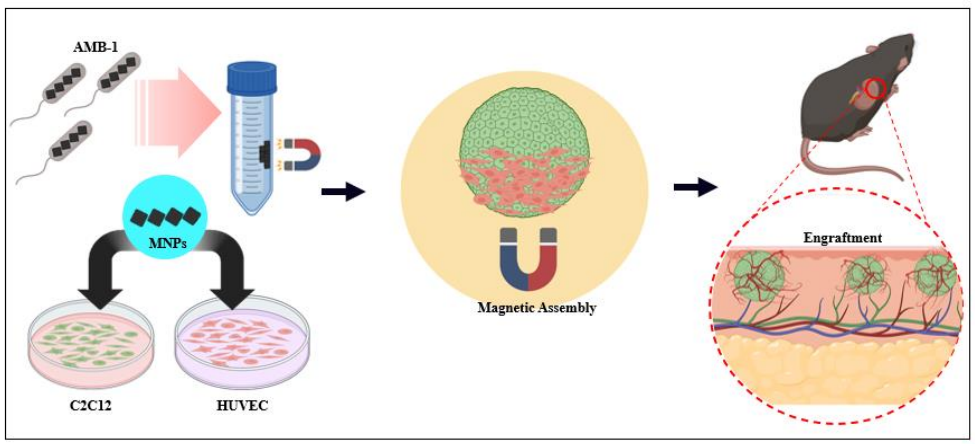

[Figure 1] Representative scheme of engraftment with endothelial cells around spheroids using magnetic assembly system.

Chapter 2. Vascularization of the Assembly Fabricated in the Magnetic System

2.1. Material and Method

2.1.1 MNP preparation

MNPs were extracted from one of the types of Magnetotactic bacteria, Magnetospirillum magneticum; AMB-1 strain. The culture meida of AMB-1 was produced based on the composition of ATCC medium: 1653 Revised Magnetic spirillum growth Medium (MSGM) that used after autoclave sterilization. AMB-1 was filled with media to prevent air in 50ml conical tubes and pre-cultured overnight at 24℃ in the shaking incubator. Fermenter was cleaned thoroughly, and 3L of MSGM was added to sterilize the whole with autoclave and used when the media cooled sufficiently. Since AMB-1 is an anaerobic organism, nitrogen gas was injected into the fermenter for 30 minutes to remove all oxygen in the media. The fermenter was set at 150 rpm, 26℃, and pH was maintained 6.75 using ATCC feeding solution (acid) and NaOH (base). Pre-cultured AMB-1 was put in the fermenter using 50 ml syringe and main culture was conducted by observing changes in temperature and pH for about 2 weeks until feeding solution does not decrease.

The culture-completed AMB-1 was moved to 500 ml silicon tubes with MSGM, and ultracentrifuge was performed under conditions of

7000 rpm, 20 min, and 4℃. The resulting pellet was resuspended in about 4 ml DPBS using vortex mixer. When the pellet was suspended, cell membrane lysis was proceeded with ultrasonicator (pulse; 2s/2s, time; 15min, Ampl; 35%). MNPs were collected by neodymium magnet under 100 mm culture dish with racking until there was no gathering around the magnet. The collected MNPs were washed using DPBS in the same way as collection until the DPBS became transparent excluding MNPs. MNPs were dissolved in 5 ml of DPBS and sterilized with autoclave. MNPs were quantified as Fe ions by ICPS and diluted to 1 mg/ml in DPBS and stored as 1 ml stocks at 4℃.

2.1.2 Cell culture

Human umbilical vein endothelial cell (HUVEC) was purchased from Lonza and used passage 3-7 for assay. The culture media was used by adding 1% penicillin/streptomycin (P/S; Gibco, cat. 15140122) to the Endothelial cell Growth medium 2 (EGM-MV2; Promocell, Cat. C-22011) and subculture was performed by diluting the 0.25% trypsin-EDTA (Gibco, cat. 25200-114) solution five times with Dulbecco's phosphate buffered saline (DPBS; Biowest, cat. L-0615). HUVECs were cultured in 6 well plate (SPL, cat. 30006) at 37℃ under 5% CO_2 with humidity.

Mouse myoblast C2C12 cells were cultured within high-glucose Dulbecco's modified Eagle's medium (DMEM; Hyclone, cat. SH30243.01) including 10% fetal bovine serum (FBS; Corning, cat. 35-015-CV), 1% P/S and subculture was performed with 0.05%

trypsin-EDTA. C2C12 cells were cultured in 6 well plate at 37℃ under 5% CO_2 with humidity.

Each cell was changed their media every 2 days. When subculture was performed, all cells were collected by centrifuge under conditions of 1100 rpm, 5 min, 25℃.

2.1.3 Transmission Electron Microscope (TEM)

MNPs were washed with DPBS while holding MNPs using a neodymium magnet. Collected MNPs were diluted by 100 times with DPBS. A drop of diluted MNPs were added onto a TEM grid and were dried in a 60℃ oven for 2 hours. Imaging of MNPs was done using a 200kV TEM (JEM-2100(JEOL Ltd, Japan)). 10% SDS treated on MNPs for 5 hours at 90℃ for removing lipid layer of MNPs. SDS-treated MNPs were obtained in the same way of non-treated MNPs. Size distribution was measured as diameter of MNPs on TEM image by image J.

2.1.4 Physical Property Measurement System (PPMS)- Vibrating Sample Magnetometer (VMS)

MNPs in DPBS were washed with DW by centrifugation at 3000 rpm, 5 min, 5 times. MNPs were lyophilized to make dry form. Dried MNPs were performed PPMS-VSM analysis (PPMS-14(Quantum Design, USA) to measure their magnetization at range from -1000 Oe to 1000 Oe.

2.1.5 Prussian Blue staining

Prussian blue staining was conducted to stain and quantify the MNPs in cells. After conducting CCK8 assay, cells in a 96-well plate were washed twice with DPBS and fixed with 100 μL of 2% PFA overnight at 4℃. Cells were washed again with PBS twice and permeabilized by adding 100 μL of 0.525% Triton-X in DPBS and incubating at room temperature for 10 minutes with shaking. Permeabilized cells were washed twice with DPBS. 100 μL of 4 v/v% HCl in distilled water and 4 w/v% potassium ferrocyanide (Sigma) in distilled water mixed in a 1:1 volume ratio was added to each well. A staining was done by incubating a plate at room temperature for 20 minutes with shaking. Cells were washed twice with DPBS for the last time, and 100 μL of DPBS was added to each well for quantification. Absorbance was measured at 700 nm via plate reader for quantification of stained MNPs. As the seeding density is uniform, normalization of the amount of cell was not necessary for this assay. For imaging Prussian staining of internalized MNPs, Hematoxylin was used as counter stain to clearly obtain in images.

2.1.6 Inductively Coupled Plasma Atomic Emission Spectrometer (ICPS)

Cellular internalized MNPs were measured as Fe ions quantification by ICPS. Each cell which incubated with 0-50 μg/ml of MNPs for 24 h was trypsinized and collected by centrifuge. Collected cell pellets were reacted with 1 ml of HCl for 2 h at 60℃ and 9 ml of DW was added to stop the reaction. Diluted solution was

filtered with 0.45 μm pore size. Filtered solution was analyzed as Fe ions by ICPS and the data were calculated with dilution time and cell number.

2.1.7 Cell counting kit (CCK8) assay

Dojindo CCK8 assay was used to assess the cytotoxicity caused by MNP. The CCK8 solution used in the assay was stored at 4℃ and was used within a year of purchase. Each cell line was seeded into a 6-well plate and was provided with 2 mL of cell culture medium. Cells were grown until its confluency was 60%-70%. MNPs with six concentrations - 0 μg/mL, 10 μg/mL, 20 μg/mL, 30 μg/mL, 40 μg/mL, and 50 μg/mL - were introduced to each well containing 2 mL of fresh cell culture medium. Six groups of cells containing six different concentrations of MNPs were incubated for 24 hours in a 37℃ incubator with 5% CO2. Each group of cells was trypsinized, and cell numbers were counted using a hemocytometer. Same number of cells that composite 80% confluency in 100 μL of fresh medium was seeded into five wells of a 96-well plate. In addition to six groups of cells, blank medium without any cell was added to five well of a 96-well plate. A 96-well plate containing blank medium and six groups of cells was incubated for another 24 hours in a 37℃ incubator with 5% CO2. Once cells adhered to the bottom of a well plate, 10 μL of CCK-8 solution was added to each well and incubated for 2 hours in a 37℃ incubator with 5% CO2. After incubation, 100 μL solution from each well was dispensed into a new well and measured the absorbance at 450 nm via plate reader.

The survival rate for each group of cells containing different MNP concentration was calculated using three absorbance values after excluding the maximum and the minimum values. The survival rate was calculated as follows:

$$\frac{Absorbance_{sample} - Average\ Absorbance_{blank}}{Average\ Absorbance_{negative\ \ control} - Average\ Absorbance_{blank}}$$

where a negative control is a group of cells with 0 μg/mL.

2.1.8 Real time polymerase chain reaction (RT-qPCR)

RT-qPCR was conducted to confirm the gene expression in cells in their two-dimensional and three-dimensional states. Membrane lysis was done by incubating sample cells in 2D and 3D with 500 μL of Trizol reagent for 5 minutes at room temperature. Cells in Trizol reagent were stored at -80℃ and thawed when conducting RNA extraction. To dissolve RNA, 200 μL of chloroform was added to the cells in 500 μL Trizol reagent. The solution was vortexed mildly and incubated at 4℃ for 3 minutes. After incubation, microcentrifugation at 12000 rpm for 15 min at 4℃ results in a phase separation. 200 μL of the uppermost transparent aqueous solution was collected, and 500 μL of isopropanol was added. Solutions were mixed thoroughly by inverting a tube and were incubated for 10 minutes at 4℃ for precipitation. RNA pellet was collected after microcentrifugation at 12000 rpm for 20 min at 4℃. After removing the supernatant, 1 mL of 75% ethanol was added to

wash the RNA pellet. RNA pellet in 1 mL of 75% ethanol was centrifuged at 8000 rpm for 5 min at 4℃ to obtain RNA. The supernatant was removed, and RNA was dried. RNA was resuspended in 20 μL of DEPC water and were denatured by incubating in a heat block at 58℃ for 15 minutes. After measuring the RNA concentration and mixing the correct amount with DEPC water, cDNA could be synthesized by mixing dNTP, RT buffer, Reverse Transcriptase, RNase inhibitor, and random hexamer. qPCR was conducted by mixing cDNA with primer and SYBR green. Each gene expression was normalized by hGAPDH or mGapdh.

2.1.9 Live and dead assay

The spheroids or assemblies were washed with DPBS before staining. And they were incubated in live and dead solution for 30 min at 37℃. Live and dead solution was composited with 0.5 μl/ml of Calcein-AM and 2 μl/ml of EthD-1. Stained spheroids or assemblies were washed with DPBS twice. Bright field and fluorescent image was obtained by EVOS 2(EVOS® FL Auto 2 Cell Imaging System).

2.1.10 Magnetic spheroid formation

C2C12 in a 6-well plate was incubated with 20 μg/mL MNP in 2 mL of medium for 24 hours. Cells were washed twice with DPBS and were incubated in medium for another 24 hours for stabilization. After washing with DPBS, 0.05% EDTA-trypsin was used to suspend the cells, which were collected by centrifugation at 1100

rpm for 5 min at 25℃. 5000 cells per well were seeded into a round bottom ULA 96 well plate, and a round shaped-neodymium magnet was placed beneath each of the ULA round-bottom well. Cells were cultured for 48 hours to form spheroids. 2% paraformaldehyde (PFA) was treated to formed C2C12 spheroids for 15 min to inhibit unexpected sprouting ability of C2C12 after they were assembled. They were washed with DPBS 3 times for 10 min to remove extra PFA and stored at 4℃. When magnetic assembly was performed, the fixed spheroids which had been stored cold was incubated at 37℃ above 30 min and washed with culture media just before use.

2.1.11 Magnetic assembly

HUVECs were incubated for 24 hours in a 6-well plate supplemented with 2 mL of medium containing 20 μg/mL MNP. Cells were washed twice with DPBS and were incubated in medium for 24 hours for stabilization in a 37℃ incubator with 5% CO2. After washing, cells were trypsinized by using 0.05% EDTA-trypsin and were collected via centrifugation at 1100 rpm for 5 minutes at 25℃. 5000 HUVEC cells per spheroid were added to fixed C2C12 spheroids and were cultured for 24 hours in the presence of neodymium magnets to form an assembly in the same way of spheroid formation.

2.1.12 Sprouting assay

Fixed C2C12 spheroids with dissociated HUVECs or with assembled HUVECs were placed on Matrigel. The same amount of

5,000 HUVECs were used in both the dissociated and assembled groups. Spheroid with dissociated HUVECs was obtained at 24 h and assembly was obtained at 24 h, 48 h, and 72 h. The images sprouting assembly were analyzed by Wimsprout.

2.13 Animal experiment – Engraftment on mouse kidney

The spheroids and assemblies were washed with DPBS and transplanted into the subcapsular membrane of the kidney. Eight-week-old C57BL/6J mice (Narabiotech, Korea) were used for spheroid or assembly transplantation. Each mouse was anesthetized intraperitoneally by a 4:1 mixture of alfaxalone (DEC007, Careside, Korea) and rompun (192492, BayerKorea, Korea), and its hair was removed. After a small incision, a left kidney was extruded, and a small scratch was made on the kidney using a needle to secure the room for transplants. 24 spheroids or assemblies were inserted into the subcapsular membrane of the kidney with 10 μL of DPBS. After 3 days, mice were sacrificed with CO2, and the kidney was fixed with 4% PFA for 24 h at 4℃.

2.14 Animal experiment – Murine ischemia model

Eight-week-old BALB/c-nu mice (Narabiotech, Korea) were used for the hindlimb ischemia model. Each mouse was anesthetized intraperitoneally by a 4:1 mixture of alfaxalone and rompun. A small incision was made on the mouse's thigh skin to reveal the femoral artery. Two parts of the femoral artery were ligated with a suture, and the artery was cut with a Bovie cautery pen (HIT1, Bovie

Medical Corporation, USA) to induce hindlimb ischemia. The spheroid and assembly groups were transplanted by intramuscular injection using a catheter tube. In the case of the sham group, only DPBS was injected. 150 spheroids or assemblies in 200 μL of DPBS were transplanted per mouse. The degree of necrosis of the legs was compared on the 0th, 1st, 3rd, and 7th days after respiratory anesthesia with isoflurane.

2.15 Immunohistology

Immunohistology of fixed tissue was done by cryo-sectioning. The tissue cut by the microtome was stained on the glass slide. Anti-mouse (ab182981, Abcam, UK) and human CD31 (303101, Biolegend, UK) were stained with 594 nm and 488 nm fluorescent respectively.

2.16 Statistical analysis

Experiments were performed at least in triplicate for statistical analysis. T-test was used for a statistical analysis of PCR data, and one-way ANOVA was used for other data from GraphPad Prism version 9.4.1.

2.2. Result and Discussion

2.2.1. Characteristics of magnetic nanoparticles

The materials used in all experiments were magnetic nanoparticles extracted from *Magnetospirillum sp.* [23, 26, 27]. AMB-1 and collected with magnets [15, 34, 36, 37]. TEM analysis of MNPs showed the shape and size of MNPs from AMB-1 **(Figure 2A)** [38]. MNPs had cubic shapes with about 40-50 nm uniformed diameters **(Figure 2C)** [24, 30]. MNPs were encapsulated by a thin out-layer that had a thickness of about 2-3 nm. The magnetic nanoparticles, derived from the magnetotactic bacteria, are also called magnetosomes because the surface of the particles produced in the body is encapsulated with a thin lipid layer like other organelles. Because of this lipid layer, MNPs from bacteria have properties of biocompatibility and spontaneous internalization into various cells [29]. To confirm the outer layer of MNPs obtained on TEM data consisted of lipids, the isolated MNPs were treated with 10% SDS known as a lipid detergent **(Figure 2B)** [39-41].

PPMS-VSM analysis indicated the magnetization of MNPs from AMB-1. There are three representative magnetization types, paramagnetism, superparamagnetism, and ferromagnetism [42]. The magnetization pattern of MNPs showed lagged curve called a hysteresis loop **(Figure 2D)** [31, 43]. Hysteresis of magnetization means ferromagnetism which refers to the property of magnetizing

even in the absence of an external magnetic field. The morphology and magnetization pattern of MNPs used in this study were the same as the well-known properties of magnetosomes.

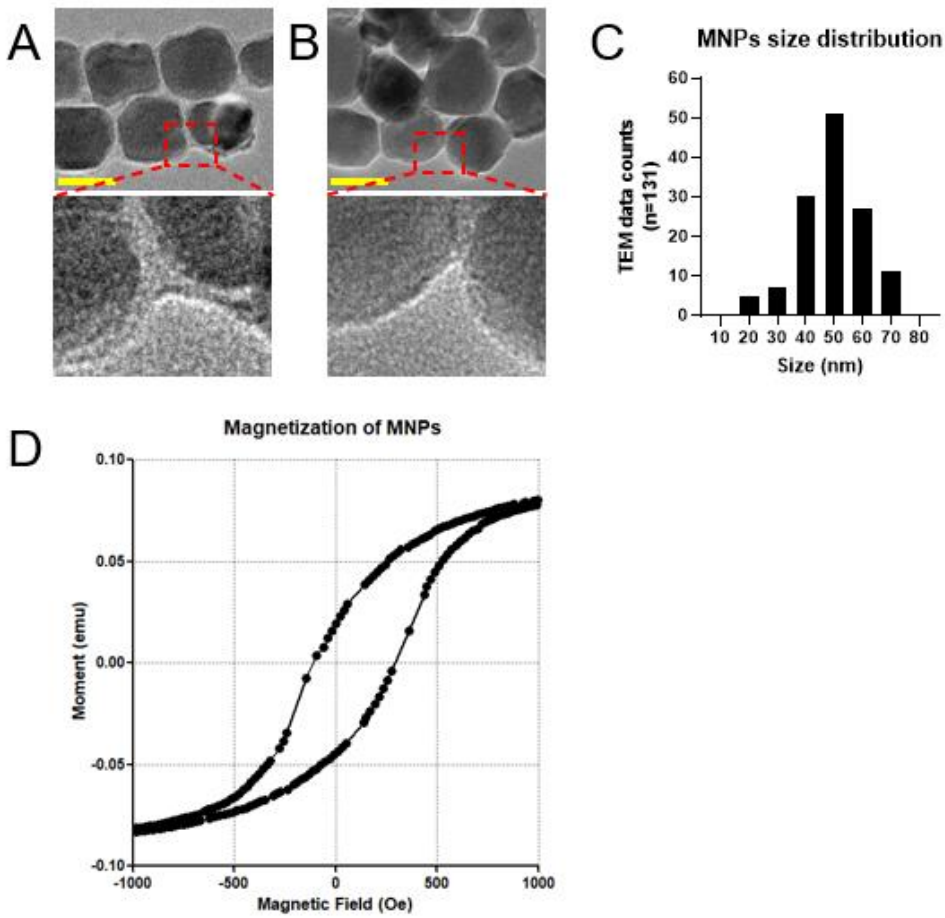

[Figure 2] Characteristics of magnetic nanoparticles.
(A, B) TEM images of magnetic nanoparticles extracted from AMB-1. (A) Normal MNPs with thin lipid layer. (B) Lipid layer removed MNPs by 10% SDS. (Scale bar, 50 nm) (C) Size distribution of MNPs from TEM data. (Analyzed by image J) (D) Magnetization of magnetic nanoparticles in magnetic field ±1000 Oe.

2.2.2. Effects of magnetic nanoparticles on 2D cells

Internalization of MNPs on cells.

Internalized MNPs on cells were detected by Prussian blue staining which stains metallic ions to blue color **(Figure 3A, B)**. Cells were incubated with MNPs for 24 h and washed twice by DPBS for staining. In Prussian blue images, blue colors populated in cytosol avoiding the nucleus of each cell [44-46]. And there were increased tendencies of MNPs in the cytosol as treated MNPs concentration increased. The cellular morphology could be clearly distinguished due to stained cytosol as the concentration of MNPs increased. There were some similar increasing patterns on absorbances at 700 nm of Prussian blue staining normalized by 10 μg/ml **(Figure 3C, D)**. Similarly, when quantifying the amount of Fe ions per cell through ICPS, it could be seen that it tends to rise with MNPs concentrations **(Figure 3E, F)**. It indicated MNPs from AMB-1 were spontaneously internalized into cells and the amount of MNPs in cells was controlled by concentrations of treated-MNPs.

Cytotoxicity of MNPs on cells.

CCK8 assay was used to confirm the viability of cells with MNPs [36, 37]. Each cell was incubated with MNPs of 0-50 μg/ml concentration for 24 h and reseeded in a 96-well culture plate to test the survival rate. CCK solution for detecting the proliferation of cells was added after 24 h from cell seeded. Cells were incubated at

37℃ with CCK reagent for 2 h reaction. Culture media with CCK solution was moved to empty wells because of absorbance interruption by MNPs and measured absorbances at 450 nm. The absorbances excluded blank value were normalized by control concentration, 0 μg/ml of MNPs. There were no significant differences according to concentrations **(Figure 4)**. There are some studies that internalized MNPs enhance the growth of host cells by ROS [47-49]. Similarly, this CCK data also showed higher viabilities at low concentrations of MNPs, 10 μg/ml of MNPs on HUVEC **(Figure 4A)** and 20 μg/ml of MNPs on C2C12 **(Figure 4B)**. A little decrease of viability was detected above 30 μg/ml concentration of MNPs on HUVEC, so 20 μg/ml of MNPs was decided as the treating concentration.

Effects of MNPs on cellular functionalities.

The functionality of MNPs was evaluated by RT-qPCR. The vascularization ability of HUVEC is the most important for the engraftment of the assembly after transplantation. Therefore, we tried to find out whether the internalization of MNPs causes a change in HUVEC's function of vascularization. Since the purpose of assembly with HUVEC is to actively vasculogenesis rather than passive angiogenesis, the analysis of gene expression of receptors for angiogenic factors and molecules about adhesion was focused on [50]. Vasculogenic gene expressions were analyzed, including Vascular endothelial growth factor receptor 1 (*VEGFR-1*; *FLT1*),

Vascular endothelial growth factor receptor 2 (*VEGFR-2*; *KDR*), and Angiopoietin-1 receptor (*TEK*; *TIE2*) **(Figure 5A-C)**. There was little increase in *FLT1* and *TIE2* gene expression but no significant difference according to the presence of MNPs. And there was a significant increase in gene expressions with KDR. In adherent molecules gene expressions, including Platelet endothelial cell adhesion molecule (*PECAM1*; *CD31*), Gap junction alpha-1 protein (*Cx43*), and Integrin beta-1 (*ITGB1*) **(Figure 5D-F)**. PCR data indicated that internalized MNPs did not decrease the vascularization functionalities of HUVECs.

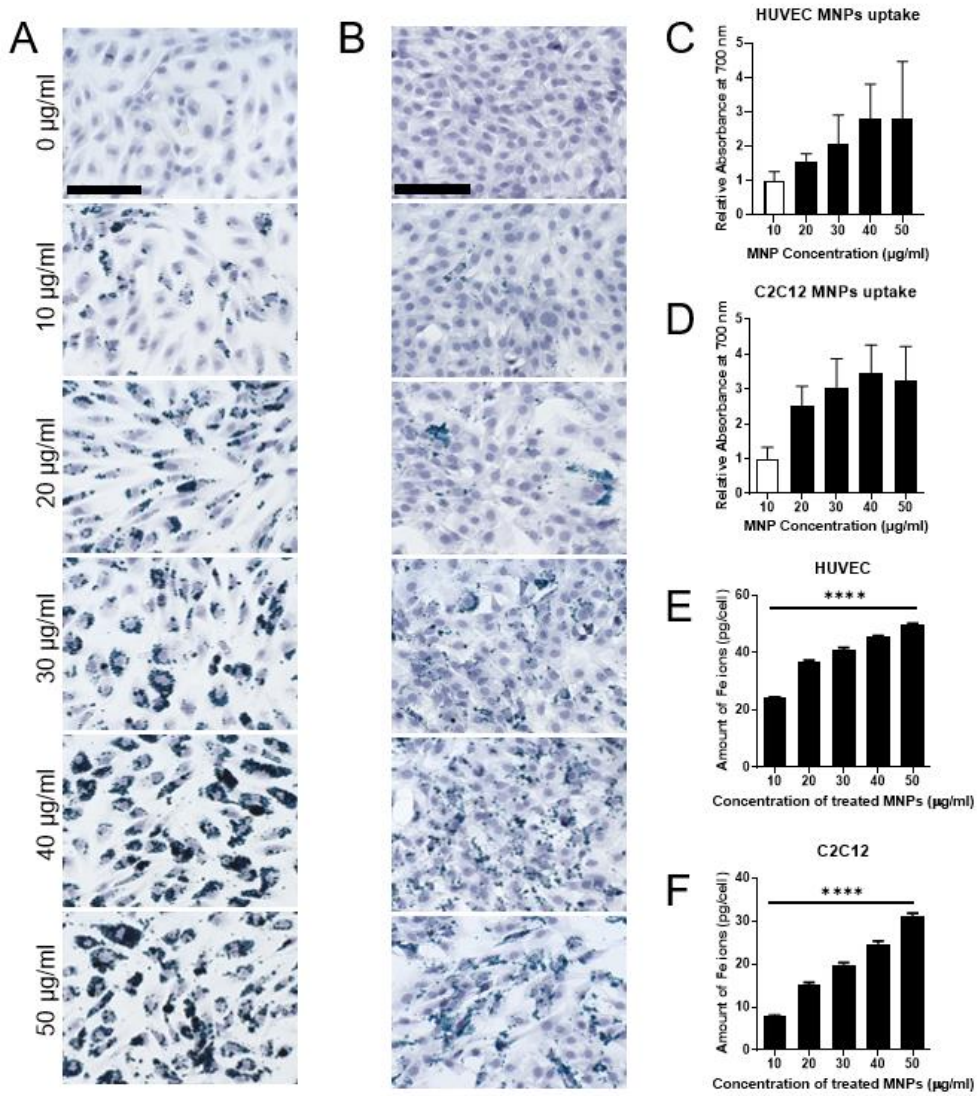

[Figure 3] Cellular internalization of MNPs.

(A, B) Prussian blue staining images of magnetic nanoparticles treated cells. (A) MNPs treated HUVEC by 0−50 μg/ml concentration in sequence. (B) MNPs treated C2C12 by 0−50 μg/ml concentration in sequence. (Scale bar, 100 μm) (C, D) Relative absorbance at 700 nm of Prussian blue stained cells normalized by absorbance of 10 μg/ml MNPs concentration. (E, F) Amount of Fe ions in each cell analyzed by ICP−AES. (**** indicated p<0.001)

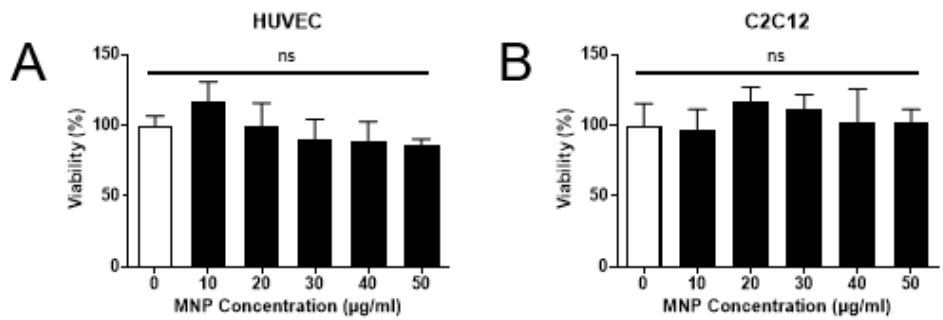

[Figure 4] Cytotoxicity of MNPs on cells.
(A, B) Cytotoxicity of internalized MNPs according to 0−50 μg/ml concentrations analyzed by CCK8 assay. (A) Viability on MNPs internalized HUVEC. (B) Viability on MNPs internalized C2C12.

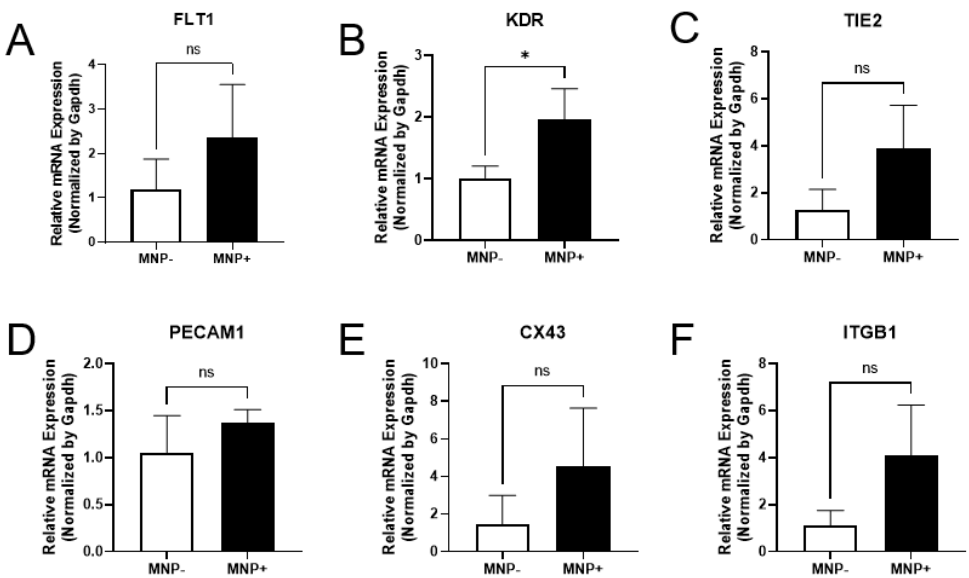

[Figure 5] Functionality analysis of MNPs internalized endothelial cells by RT-qPCR.

(A-F) Effects on endothelial functional gene expression of MNPs. (A-C) Change of vascularization-related gene expressions. (D-F) Change of adhesive molecules gene expressions. (Normalized by GAPDH. * indicated $p<0.05$)

2.2.3. Magnetic nanoparticles induced 3D assembly

Magnetic spheroid formation with MNPs.

To form spheroid of C2C12 cells, C2C12 cells were incubated with 20 μg/ml of MNPs for 24 h and incubated in fresh media for 24 h to be stabilized after twice washing with DPBS. Cells were seeded on a round bottom ultra-low attachment 96-well plate for 5000 cells/well with round shape neodymium magnet under the bottom **(Figure 6A)**. The spheroids were formed after 48h from seeding. Magnetic-formed spheroids seemed darker because of the internalized MNPs **(Figure 6B)**. The viability of MNPs-internalized cells in 3D spheroid was evaluated by live/dead assay. Calcein-AM refers to green fluorescence and indicates live cells while EthD-1 refers to red fluorescence and indicated dead cells. Magnetic spheroid had a black core even in live/dead image that proved there were MNPs inside. We wondered if spheroid with MNPs too high compaction inducing hypoxia inside had [51]. There was no significant difference in gene expressions of cell-to-cell adhesion molecules, including Gap junction alpha-5 protein (Connexin 40; *Cx40*) and Gap junction gamma-1 protein (Connexin 40; *Cx45*), between spheroid with or without MNPs **(Figure 6C, D)**. And Hypoxia-induced factor 1-α (*Hif1-*α) was not showed a significant increase in magnetic spheroid formation **(Figure 6E)**. There was not much compaction and induced hypoxia that was harmful to spheroids in RT-qPCR data.

Magnetic 3D assembly with MNPs.

Since the magnetic C2C12 spheroid was designed to represent various cell therapeutics including spheroids or organoids, it was intended to block individual abilities. Especially, because C2C12 has the property of extending to the surroundings, it was not possible to confirm the sprouting effect of HUVEC alone by the assembly, so its unexpected sprouting was blocked by fixation using FPA [52]. The residue of PFA could be completely removed by washing using magnets (Figure 7B) [35]. HUVECs were incubated with MNPs at 37℃ for 24 h in a 6-well plate. They were washed twice with PBS for removing suspended MNPs and incubated in fresh media for stabilization and removing MNPs that were not internalized in cells but just attached to the cell surface. HUVECs were added on C2C12 spheroids for 5000 cells/spheroid. Magnetic assembly was performed in the same way as magnetic spheroid formation, on the round bottom ULA 96-well plate with the magnet under the bottom. HUVECs were assembled around C2C12 spheroid for 24 h (Figure 7A). To confirm the cytotoxicity of fixed spheroid to HUVECs, live/dead assay was applied to the assembly. Fixed C2C12 spheroids seemed red with death, while HUVECs assembled around spheroid seemed green with life (Figure 7C). Due to the internalization of MNPs, the core of the assembly seemed dark, so the red fluorescence was not sufficiently detected. For this reason, it seems that a certain amount of fluorescence was expressed in

assembled alive HUVECs by strengthening the intensity of fluorescence.

Sprouting functionality of assembly.

Spouting assays were used to confirm whether MNPs-internalized HUVECs stretched and formed blood vessels after assembly [53, 54]. Spheroids and dissociated HUVECs were seeded on Matrigel in vitro to evaluate whether they would be engrafted even when HUVECs were simply added, not assembled. When HUVECs were dissociated, blood vessels were randomly formed instead of directly connecting the spheroid to help the engraftment **(Figure 8A)**. In this case, it is judged that HUVEC made tube formation rather than spouting. On the other hand, assembled HUVECs were located around the spheroid even after seeding, extending blood vessels into the Matrigel over time **(Figure 8B, C)**. Assembly showed that the sprouting blood vessels were in contact with the spheroid and that the sprouting length is significantly different within 3 days **(Figure 8D)**. Sprouting area and length on microscope images according to days were analyzed by Wimsprout.

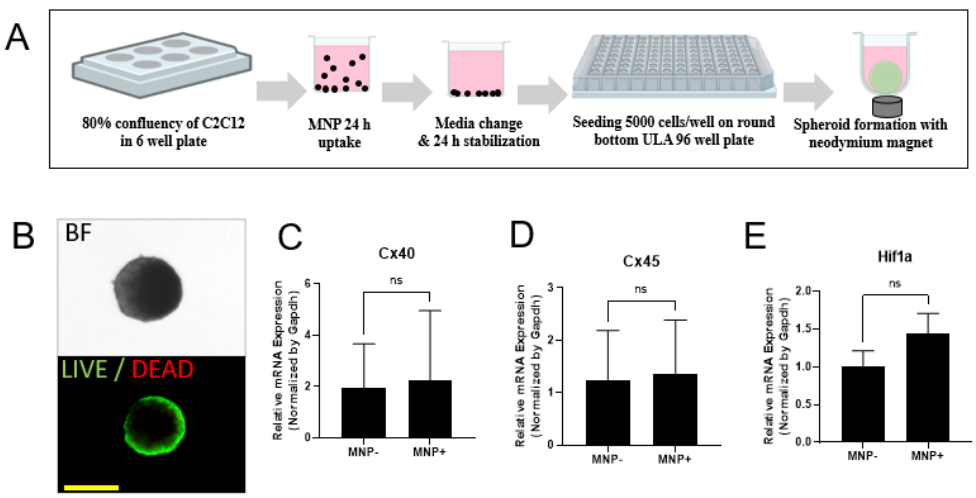

[Figure 6] Magnetic spheroid formation of C2C12.
(A) Method scheme of magnetic spheroid formation system. (B) Bright field microscope image (BF) and live and dead assay image of fabricated C2C12 spheroid. (Scale bar, 275 nm) (C-E) Change of compaction relative gene expressions. (Normalized by Gapdh)

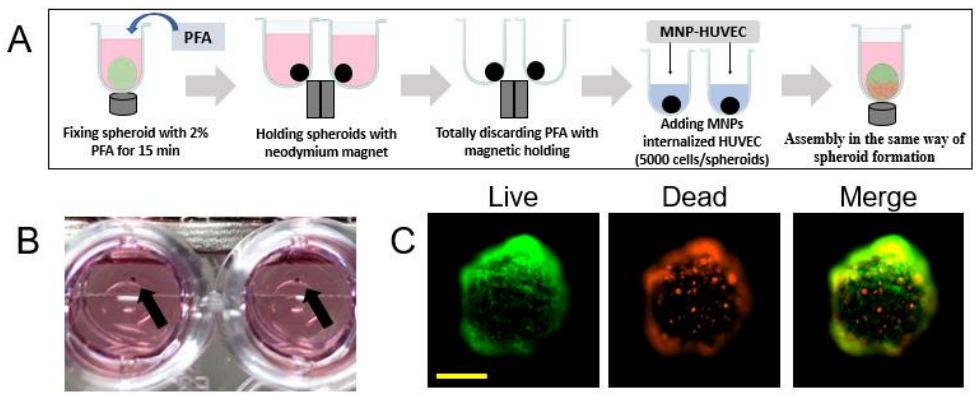

[Figure 7] Magnetic assembly with HUVEC.
(A) Method scheme of magnetic assembly system. (B) Image of C2C12 spheroids being pulled towards the magnet for washing. (C) Live and dead image of assembly after PFA fixation of C2C12 spheroid. (Scale bar, 125 nm)

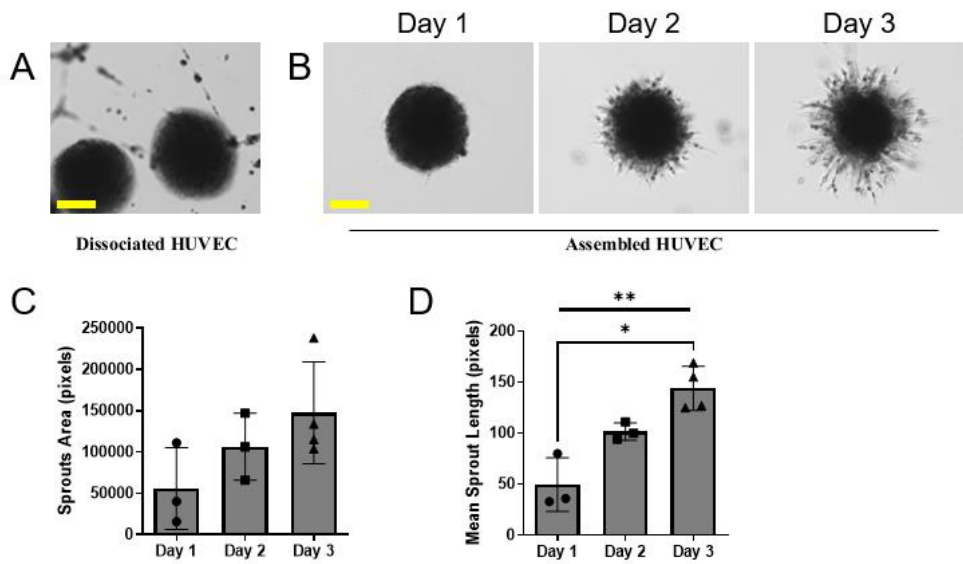

[Figure 8] Sprouting functionality of assembly.
(A) Microscope image of C2C12 spheroid with dissociated HUVEC on Matrigel. (B) Microscope images of sprouting assembly according to days. (Scale bar, 125 nm) (C, D) Evaluations of sprouting ability of magnetic assembly analyzed by Wimsprout. (* indicated $p<0.05$, ** indicated $p<0.01$)

2.2.4. Vascularization of assembly for engraftment *in Vivo*

Engraftment of assembly on mouse kidney.

To obtain the rapid engraftment of the assembly, it was transplanted into a mouse. Transplantation for treatment must be carried out quickly within 3 days to be advantageous for the survival and function of the transplants [18-20]. To check the degree of individual engraftment without forming a cluster between assembly members, the assembly was carried out into the subcapsular membrane of the kidney, a place that can be easily identified from the outside and separated individually **(Figure 9A)** [14]. The mice were sacrificed after 3 days of transplantation. In the histological image of the transplanted assembly with hematoxylin staining, the morphology of fixed C2C12 spheroids was observed accurately (red circle), and the morphology of sprouting HUVECs inside kidney was also observed (blue arrow) **(Figure 9B)**. In the histological image, MNPs were completely distinct from other tissue components. In immunostaining, the morphology of the MNPs-internalized spheroid was identified, and the surrounding vascular network was detected. In the image of immunostaining with anti-mouse and human CD31 which refers to vessels, it was obtained that the blood vessels of the mouse, which is the host, and the blood vessels of the human which were transplanted, were connected to form a network **(Figure 9C)**. It was also observed that HUVECs were surrounded by spheroids. The connection between

host vessels and HUVECs is seemed advantageous for the transplants to supplement the elements necessary for survival and function.

Vascularization of assembly in ischemia model.

The hindlimb ischemia model was used to evaluate the vascularization ability of assembly. Two sites of the femoral arteries were tied with a suture to prevent excessive bleeding, and the femoral artery was cut with a Bovie cautery pen to induce hindlimb ischemia **(Figure 10A)** [55, 56]. The same number of magnetic assemblies or spheroids was inserted with 200 μl of DPBS in the mouse by intramuscular injection. In the case of a needle, the pressure applied to the spheroids or assemblies during injection was strong, so a blood vessel catheter was used for the transplant. The degree of leg necrosis between groups according to dates was compared by minimizing the immune response through nude mice **(Figure 10B)**. Compared to sham and spheroid groups, mice transplanted with assembly were confirmed to be relatively prevented from necrosis, proving the vascularization ability of assembly. The mice transplanted with spheroids were found to be more severe necrosis than sham group, which was expected to be an immune or inflammatory reaction.

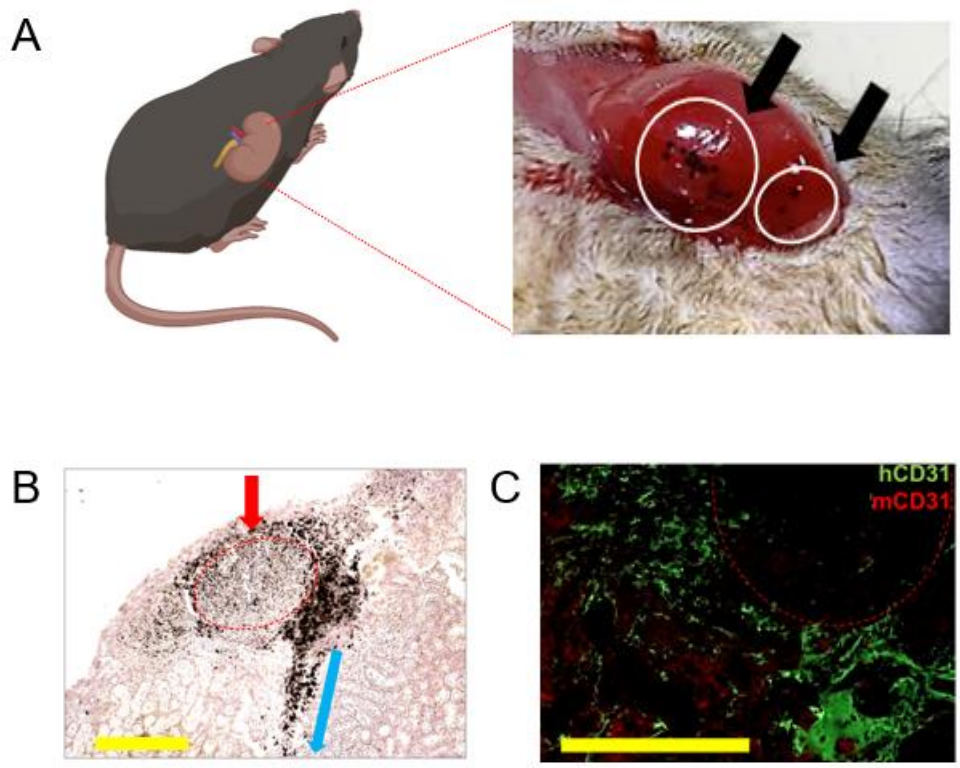

[Figure 9] Rapid engraftment of assembly on mouse kidney.
(A) Image of magnetic assemblies transplanted into subcapsular membrane of mouse kidney. (B) Tissue with hematoxylin staining indicating sprouting HUVECs. (C)Immunostaining of transplanted assembly with anti-mouse and human CD31. (Scale bar, 200 μm)

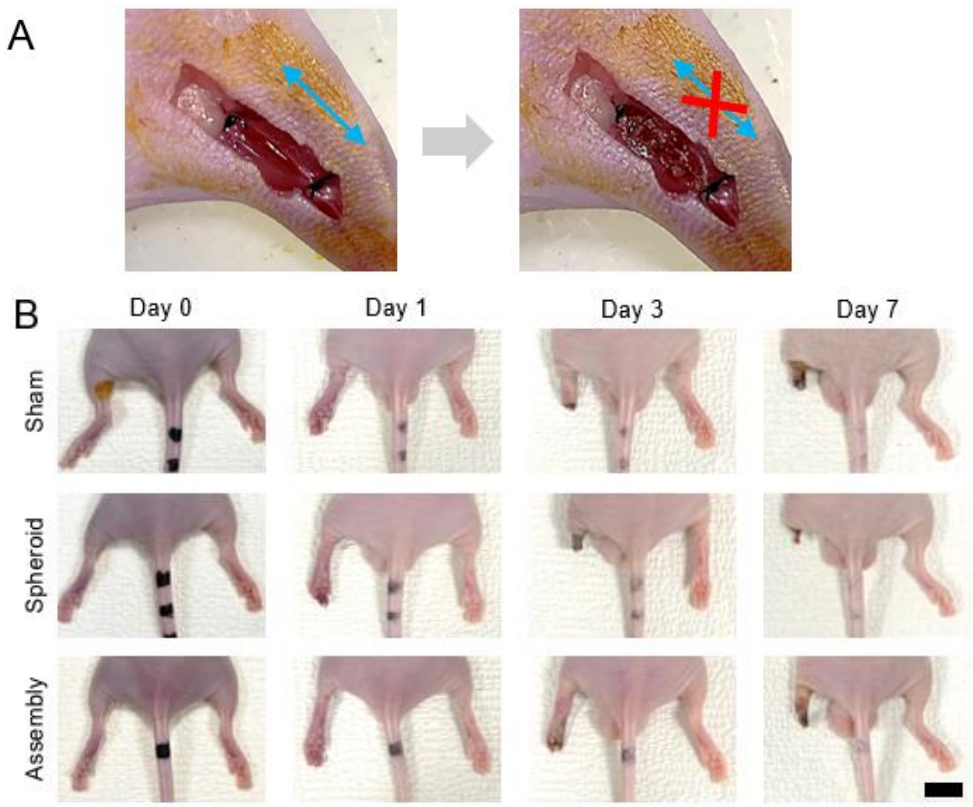

[Figure 10] Vascularization of assembly in hindlimb ischemia.
(A) Image of method for inducing hindlimb ischemia. (B) Image of hindlinb ischemia BALB/c-nu with necrosis according to time. (Scale bar, 1 cm)

Chapter 3. Conclusion

In this study, MNPs extracted from AMB-1, a species of MTB, were used to assemble myoblast spheroid with endothelial cells and applied for vascularization after transplantation. MNPs were endocytosed into cells without adversely affecting the survival and function of cells, allowing the cell to have a magnetic property. In order to generate a universalized organoid, C2C12 spheroids formed in this magnetic system were fixed with PFA to block individual specifications and advocate universal cell therapeutics. Assembly made with the magnetic system was viable despite the fixation of spheroids and showed sprouting ability on Matrigel. In addition, assembly was quickly engrafted on the murine kidney within 3 days, and functionality of vascularization was proved through the reduction of necrosis in the hindlimb ischemic mice **(Figure 9 and 10)**. Since MNPs are spontaneously uptaken by cells, there is a difference in internalization efficiency depending on the cell type [29, 30]. If cells can be uniformly magnetized, the magnetic assembly system can be applied to various cell therapies. Additionally, by incorporating studies that regulate immune responses, the system will provide clues to address both issues of immunity and vascularization. In this study, the universal applicability was confirmed through fixed spheroids, so subsequent studies will need to investigate whether long-term survival and function can be achieved using various organoids instead of fixed

spheroid. Cell recruitment through magnetic force is expected to be used in addition to strategies for regulating immune response using surface modification, which are currently being actively studied. In particular, this magnetic assembly system is expected to be a powerful platform for immune blocking and vascularization for the development of diabetes treatments [14].

References

[1] W. Kim, Y. Gwon, S. Park, H. Kim, J. Kim, Therapeutic strategies of three-dimensional stem cell spheroids and organoids for tissue repair and regeneration, Bioactive Materials 19 (2023) 50-74.

[2] I.R. Calori, S.R. Alves, H. Bi, A.C. Tedesco, Type-I Collagen/Collagenase Modulates the 3D Structure and Behavior of Glioblastoma Spheroid Models, ACS Applied Bio Materials 5(2) (2022) 723-733.

[3] Y. Park, C.K. Franz, H. Ryu, H. Luan, K.Y. Cotton, J.U. Kim, T.S. Chung, S. Zhao, A. Vazquez-Guardado, D.S. Yang, Three-dimensional, multifunctional neural interfaces for cortical spheroids and engineered assembloids, Science advances 7(12) (2021) eabf9153.

[4] K. Skrzypek, M. Groot Nibbelink, J. Van Lente, M. Buitinga, M.A. Engelse, E.J. De Koning, M. Karperien, A. Van Apeldoorn, D. Stamatialis, Pancreatic islet macroencapsulation using microwell porous membranes, Scientific reports 7(1) (2017) 1-12.

[5] D.T. Bowers, W. Song, L.-H. Wang, M. Ma, Engineering the vasculature for islet transplantation, Acta biomaterialia 95 (2019) 131-151.

[6] M. Khosravi-Maharlooei, E. Hajizadeh-Saffar, Y. Tahamtani, M. Basiri, L. Montazeri, K. Khalooghi, M.K. Ashtiani, Islet transplantation for type 1 diabetes: so close and yet so far away,

Eur J Endocrinol (2015).

[7] D. Hutt, Engraftment, graft failure, and rejection, The European Blood and Marrow Transplantation Textbook for Nurses (2018) 259-270.

[8] Y. Takahashi, K. Sekine, T. Kin, T. Takebe, H. Taniguchi, Self-condensation culture enables vascularization of tissue fragments for efficient therapeutic transplantation, Cell reports 23(6) (2018) 1620-1629.

[9] R. Gibly, J. Graham, X. Luo, W. Lowe, B. Hering, L. Shea, Advancing islet transplantation: from engraftment to the immune response, Diabetologia 54(10) (2011) 2494-2505.

[10] K. Yang, E.D. O'Cearbhaill, S.S. Liu, A. Zhou, G.D. Chitnis, A.E. Hamilos, J. Xu, M.K. Verma, J.A. Giraldo, Y. Kudo, A therapeutic convection-enhanced macroencapsulation device for enhancing β cell viability and insulin secretion, Proceedings of the National Academy of Sciences 118(37) (2021) e2101258118.

[11] L. Xu, K. Kanasaki, M. Kitada, D. Koya, Diabetic angiopathy and angiogenic defects, Fibrogenesis & tissue repair 5(1) (2012) 1-9.

[12] M. Zubair, F. Fatima, Molecular Mechanism and Biomechanics of the Diabetic Foot: The Road to Foot Ulceration and Healing, Diabetic Foot Ulcer, Springer2021, pp. 87-120.

[13] S.-B. Catrina, X. Zheng, Hypoxia and hypoxia-inducible factors in diabetes and its complications, Diabetologia 64(4) (2021) 709-716.

[14] M. Kim, H. Kim, Y.-s. Lee, S. Lee, S.-E. Kim, U.-J. Lee, S.

Jung, C.-G. Park, J. Hong, J. Doh, Novel enzymatic cross-linking-based hydrogel nanofilm caging system on pancreatic β cell spheroid for long-term blood glucose regulation, Science advances 7(26) (2021) eabf7832.

[15] Y.B. Lee, J.-Y. Lee, T. Ahmad, S. Bak, J. Lee, H.D. Kim, T.H. Park, N.S. Hwang, Y.M. Lim, H. Shin, Construction of 3-D cellular multi-layers with extracellular matrix assembly using magnetic nanoparticles, Journal of Biomedical Nanotechnology 12(10) (2016) 1916-1928.

[16] E.A. Lee, H. Yim, J. Heo, H. Kim, G. Jung, N.S. Hwang, Application of magnetic nanoparticle for controlled tissue assembly and tissue engineering, Archives of pharmacal research 37(1) (2014) 120-128.

[17] J.A. Kim, J.-H. Choi, M. Kim, W.J. Rhee, B. Son, H.-K. Jung, T.H. Park, High-throughput generation of spheroids using magnetic nanoparticles for three-dimensional cell culture, Biomaterials 34(34) (2013) 8555-8563.

[18] R. Coyle, J. Yao, D. Richards, Y. Mei, The effects of metabolic substrate availability on human adipose-derived stem cell spheroid survival, Tissue Engineering Part A 25(7-8) (2019) 620-631.

[19] H. Nagano, Y. Suematsu, M. Takuma, S. Aoki, A. Satoh, E. Takayama, M. Kinoshita, Y. Morimoto, S. Takeoka, T. Fujie, Enhanced cellular engraftment of adipose-derived mesenchymal stem cell spheroids by using nanosheets as scaffolds, Scientific reports 11(1) (2021) 1-12.

[20] E.L. Hubber, C.L. Rackham, P.M. Jones, Protecting islet

functional viability using mesenchymal stromal cells, Stem cells translational medicine 10(5) (2021) 674-680.

[21] M. Razavi, F. Zheng, A. Telichko, J. Wang, G. Ren, J. Dahl, A.S. Thakor, Improving the function and engraftment of transplanted pancreatic islets using pulsed focused ultrasound therapy, Scientific reports 9(1) (2019) 1-12.

[22] F. Cayabyab, L.R. Nih, E. Yoshihara, Advances in pancreatic islet transplantation sites for the treatment of diabetes, Frontiers in Endocrinology (2021) 1077.

[23] J. Li, Y. Pan, Q. Liu, H. Qin, C. Deng, R. Che, X. Yang, A comparative study of magnetic properties between whole cells and isolated magnetosomes of Magnetospirillum magneticum AMB-1, Chinese Science Bulletin 55(1) (2010) 38-44.

[24] Z.V. Novakova, I. Gasparova, L. Krajciova, M. Molcan, I. Varga, M. Timko, L. Danisovic, Effect of magnetosomes on cell proliferation, apoptosis induction and expression of Bcl-2 in the human lung cancer cell line A549, Biologia 72(5) (2017) 554-560.

[25] S. Staniland, W. Williams, N. Telling, G. Van Der Laan, A. Harrison, B. Ward, Controlled cobalt doping of magnetosomes in vivo, Nature nanotechnology 3(3) (2008) 158-162.

[26] C.T. Lefèvre, D.A. Bazylinski, Ecology, diversity, and evolution of magnetotactic bacteria, Microbiology and Molecular Biology Reviews 77(3) (2013) 497-526.

[27] U. Heyen, D. Schüler, Growth and magnetosome formation by microaerophilic Magnetospirillum strains in an oxygen-controlled fermentor, Applied microbiology and biotechnology 61(5) (2003)

536-544.

[28] D. Faivre, D. Schuler, Magnetotactic bacteria and magnetosomes, Chemical reviews 108(11) (2008) 4875-4898.

[29] J. Shin, C.-H. Yoo, J. Lee, M. Cha, Cell response induced by internalized bacterial magnetic nanoparticles under an external static magnetic field, Biomaterials 33(22) (2012) 5650-5657.

[30] P. Wang, C. Chen, C. Chen, Y. Li, W. Pan, T. Song, The interaction of bacterial magnetosomes and human liver cancer cells in vitro, Journal of Magnetism and Magnetic Materials 427 (2017) 105-110.

[31] A. Curcio, A. Van de Walle, A. Serrano, S. Prévéral, C. Péchoux, D. Pignol, N. Menguy, C.T. Lefevre, A. Espinosa, C. Wilhelm, Transformation cycle of magnetosomes in human stem cells: from degradation to biosynthesis of magnetic nanoparticles anew, ACS nano 14(2) (2019) 1406-1417.

[32] Z. Luo, H. Du, Prospect of different types of magnetic nanoparticles in stem cell therapy, Stem Cell Reviews and Reports 16(4) (2020) 675-683.

[33] Y. Gao, J. Lim, S.-H. Teoh, C. Xu, Emerging translational research on magnetic nanoparticles for regenerative medicine, Chemical Society Reviews 44(17) (2015) 6306-6329.

[34] M. Noh, Y.H. Choi, Y.-H. An, D. Tahk, S. Cho, J.W. Yoon, N.L. Jeon, T.H. Park, J. Kim, N.S. Hwang, Magnetic nanoparticle-embedded hydrogel sheet with a groove pattern for wound healing application, ACS Biomaterials Science & Engineering 5(8) (2019) 3909-3921.

[35] W.M. Guo, X.J. Loh, E.Y. Tan, J.S. Loo, V.H. Ho, Development of a magnetic 3D spheroid platform with potential application for high-throughput drug screening, Molecular pharmaceutics 11(7) (2014) 2182-2189.

[36] B. Son, J.A. Kim, S. Cho, G.-J. Jeong, B.S. Kim, N.S. Hwang, T.H. Park, Lineage Specific Differentiation of Magnetic Nanoparticle-Based Size Controlled Human Embryoid Body, ACS Biomaterials Science & Engineering 3(8) (2017) 1719-1729.

[37] B. Son, H.D. Kim, M. Kim, J.A. Kim, J. Lee, H. Shin, N.S. Hwang, T.H. Park, Physical Stimuli-Induced Chondrogenic Differentiation of Mesenchymal Stem Cells Using Magnetic Nanoparticles, Advanced healthcare materials 4(9) (2015) 1339-1347.

[38] D. Choi, B. Son, T.H. Park, J. Hong, Controlled surface functionality of magnetic nanoparticles by layer-by-layer assembled nano-films, Nanoscale 7(15) (2015) 6703-6711.

[39] Y.A. Gorby, T.J. Beveridge, R.P. Blakemore, Characterization of the bacterial magnetosome membrane, Journal of bacteriology 170(2) (1988) 834-841.

[40] K. Gru¨nberg, E.-C. Mu¨ller, A. Otto, R. Reszka, D. Linder, M. Kube, R. Reinhardt, D. Schu¨ler, Biochemical and proteomic analysis of the magnetosome membrane in Magnetospirillum gryphiswaldense, Applied and environmental microbiology 70(2) (2004) 1040-1050.

[41] F. Guan, X. Li, J. Guo, G. Yang, Ganglioside-magnetosome complex formation enhances uptake of gangliosides by cells,

International Journal of Nanomedicine 10 (2015) 6919.

[42] E.C. Devi, S.D. Singh, Tracing the Magnetization Curves: a Review on Their Importance, Strategy, and Outcomes, Journal of Superconductivity and Novel Magnetism 34(1) (2021) 15-25.

[43] M. Molčan, A. Hashim, J. Kováč, M. Rajňák, P. Kopčanský, M. Makowski, H. Gojzewski, M. Molokáč, L. Hvizdak, M. Timko, Characterization of Magnetosomes After Exposure to the Effect of the Sonication and Ultracentrifugation, Acta Physica Polonica, A. 126(1) (2014).

[44] J.-H. Sun, Y.-L. Zhang, C.-H. Nie, S.-P. Qian, X.-B. Yu, H.-Y. Xie, L. Zhou, S.-S. Zheng, In vitro labeling of endothelial progenitor cells isolated from peripheral blood with superparamagnetic iron oxide nanoparticles, Molecular Medicine Reports 6(2) (2012) 282-286.

[45] G. Dacarro, A. Taglietti, P. Pallavicini, Prussian blue nanoparticles as a versatile photothermal tool, Molecules 23(6) (2018) 1414.

[46] S. Cho, M.J. Shon, B. Son, G.S. Eun, T.-Y. Yoon, T.H. Park, Tension exerted on cells by magnetic nanoparticles regulates differentiation of human mesenchymal stem cells, Biomaterials Advances 139 (2022) 213028.

[47] K. Li, C. Chen, C. Chen, Y. Wang, Z. Wei, W. Pan, T. Song, Magnetosomes extracted from Magnetospirillum magneticum strain AMB-1 showed enhanced peroxidase-like activity under visible-light irradiation, Enzyme and microbial technology 72 (2015) 72-78.

[48] K. Li, P. Wang, C. Chen, C. Chen, L. Li, T. Song, Light irradiation helps magnetotactic bacteria eliminate intracellular reactive oxygen species, Environmental microbiology 19(9) (2017) 3638-3648.

[49] H. Chen, K. Li, Y. Cai, P. Wang, W. Gong, L.-F. Wu, T. Song, Light regulation of resistance to oxidative damage and magnetic crystal biogenesis in Magnetospirillum magneticum mediated by a Cys-less LOV-like protein, Applied Microbiology and Biotechnology 104(18) (2020) 7927-7941.

[50] A. Singh, A.K. Gaharwar, Microscale technologies for cell engineering, Springer2016.

[51] H. Tseng, J.A. Gage, T. Shen, W.L. Haisler, S.K. Neeley, S. Shiao, J. Chen, P.K. Desai, A. Liao, C. Hebel, A spheroid toxicity assay using magnetic 3D bioprinting and real-time mobile device-based imaging, Scientific reports 5(1) (2015) 1-11.

[52] D.W. Kim, I. Jun, T.-J. Lee, J. hye Lee, Y.J. Lee, H.-K. Jang, S. Kang, K.D. Park, S.-W. Cho, B.-S. Kim, Therapeutic angiogenesis by a myoblast layer harvested by tissue transfer printing from cell-adhesive, thermosensitive hydrogels, Biomaterials 34(33) (2013) 8258-8268.

[53] M. Ackermann, A.M. Pabst, J.P. Houdek, T. Ziebart, M.A. Konerding, Priming with proangiogenic growth factors and endothelial progenitor cells improves revascularization in linear diabetic wounds, International Journal of Molecular Medicine 33(4) (2014) 833-839.

[54] D.-Y. Chen, H.-J. Wei, K.-J. Lin, C.-C. Huang, C.-C. Wang,

C.-T. Wu, K.-T. Chao, K.-J. Chen, Y. Chang, H.-W. Sung, Three-dimensional cell aggregates composed of HUVECs and cbMSCs for therapeutic neovascularization in a mouse model of hindlimb ischemia, Biomaterials 34(8) (2013) 1995-2004.

[55] A. Limbourg, T. Korff, L.C. Napp, W. Schaper, H. Drexler, F.P. Limbourg, Evaluation of postnatal arteriogenesis and angiogenesis in a mouse model of hind-limb ischemia, Nature protocols 4(12) (2009) 1737-1748.

[56] H.-J. Kang, J.-Y. Kim, H.-J. Lee, K.-H. Kim, T.-Y. Kim, C.-S. Lee, H.-C. Lee, T.H. Park, H.-S. Kim, Y.-B. Park, Magnetic bionanoparticle enhances homing of endothelial progenitor cells in mouse hindlimb ischemia, Korean Circulation Journal 42(6) (2012) 390-396.

국문초록

자성 나노 입자로 유도된 혈관 내피 세포와의 어셈블리를 활용한 혈관화 연구

조직 공학적 관점에서 생착은 이식체의 생존 및 기능에 필수적이다. 유전 혹은 후천적 이유로 인해 장기의 손상이 발생하여 세포 치료제나 장기 자체를 이식하고자 할 때, 성공적인 장기간 생존을 위해서는 이식체 주변의 혈관 형성이 필수적이다. 혈관이 풍부한 환경을 조성하기 위해서는 혈관화 전략들이 필요하다. 본 연구에서는 자성 나노 입자를 활용하여 스페로이드 주변에 혈관 내피 세포를 강제로 응집하여 어셈블리를 형성하고, 이식 이후의 생착을 위한 혈관화를 도모하고자 하였다. 자성 나노 입자는 자기주성 세균의 한 종인 AMB-1에서 생추출하여, 생체적합적이면서 세포에 자발적으로 내재화된다. 본 연구에서 수많은 오가노이드 이식체를 대표하기 위해 사용된 스페로이드는 쥐 근원세포인 C2C12를 사용하였고, 생착에 이용되는 혈관 세포는 HUVEC을 사용하였다. 20 μg/ml의 자성 나노 입자를 24 시간동안 섭취한 C2C12를 둥근 바닥의 초-저부착 배양접시에서 배양하였다. 이때 바닥에 둥근 네오디움 자석을 두어 구체 형성을 2 일간 진행하였다. 형성된 스페로이드에 자성 나노 입자를 내재화한 HUEVC을 추가하고, 마찬가지 방법으로 자석을 이용해 스페로이드 주변에 응집시킨다. 자성 나노 입자를 섭취한 HUVEC이 VEGFR1, VEGFR2, TIE2를 포함한 혈관 신생 관련 유전자 발현의 저해를 보이지

않음을 확인하였다. 만들어진 어셈블리는 in vitro에서 주변으로 혈관 세포가 뻗어 나가는 생착 능력을 확인하였다. 또한 쥐의 콩팥 막으로의 이식을 통해 형성된 어셈블리가 3일 이내에 빠르게 생착됨을 확인하였고, 하지허혈 모델에 근육으로의 이식을 통해 혈관화 능력에 대한 평가를 수행하였다. 이 기술이 다양한 이식체의 빠른 생착을 위한 범용적인 기술로 활용될 것을 기대한다.

주요어 : 생착, 혈관화, 세포 응집, 자성 나노 입자, 이식, 3차원 배양, 세포 치료제
학번 : 2021-21331